

**Size-specific, scanner-independent organ dose estimates in contiguous axial and helical head CT examinations**

Kyle McMillan<sup>a</sup>, Maryam Bostani<sup>a,b</sup>, Chris Cagnon<sup>a,b</sup>, Maria Zankl<sup>c</sup>, Ali R. Sepahdari<sup>b</sup>, Michael McNitt-Gray<sup>a,b</sup>

5    <sup>a</sup>) Biomedical Physics, David Geffen School of Medicine, University of California, Los Angeles, Los Angeles, CA 90024

<sup>b</sup>) Department of Radiological Sciences, David Geffen School of Medicine, University of California, Los Angeles, Los Angeles, CA 90024

10    <sup>c</sup>) Helmholtz Zentrum München, German Research Center for Environmental Health (GmbH), Research Unit Medical Radiation Physics and Diagnostics, Ingolstaedter Landstrasse 1, 85764 Neuherberg, Germany

**Keywords: head CT, radiation dose, organ dose, Monte Carlo dose simulations**

15

20

## Abstract

25 **Purpose:** AAPM Task Group 204 introduced size-specific dose estimates (SSDE) for pediatric and adult patients undergoing body CT examinations. This investigation extends that work to head CT exams by using Monte Carlo simulations to develop size-specific, scanner-independent CTDI<sub>vol</sub>-to-organ-dose **conversion coefficients**.

**Methods:** Using eight patient models from the GSF family of voxelized phantoms, dose to the brain and lens  
30 of the eye was estimated using Monte Carlo simulations of contiguous axial and helical scans for 64-slice multi-detector CT scanners from four major manufacturers. For each patient model and scan mode, scanner-independent CTDI<sub>vol</sub>-to-organ-dose **conversion coefficients** were calculated by normalizing organ dose by scanner-specific 16 cm CTDI<sub>vol</sub> values and averaging across all scanners. Head size was measured using both  
35 geometric and attenuation-based size metrics. Head perimeter and effective diameter (ED), both geometric size metrics, were measured directly from the GSF data at the first slice superior to the eyes. Because the GSF models pixel data is provided in terms of organ identification numbers instead of CT numbers, an indirect estimate of water equivalent diameter (WED), an attenuation-based size metric, was determined based on the relationships between WED and both ED and perimeter for a sample of patient data. Correlations between CTDI<sub>vol</sub>-to-organ-dose **conversion coefficients** and the various patient size metrics  
40 were then explored.

**Results:** The analysis of the patient data revealed a best-fit linear relationship (correlation coefficient of 0.87) between ED and WED across a wide variety of patient sizes. Using this relationship along with ED determined from the GSF data, WED was estimated for each GSF model. An exponential relationship between CTDI<sub>vol</sub> normalized organ dose and WED was observed for both contiguous axial and helical  
45 scanning. For head perimeter and ED measured directly from the GSF data, an exponential relationship between CTDI<sub>vol</sub> normalized organ dose and patient size was also observed for each scan mode. For all

patient size metrics and scan modes, correlation coefficients of the exponential fits ranged from 0.92 to 0.93 and 0.73 to 0.85 for the brain and lens of the eye, respectively.

**Conclusions:** For all scan modes, strong correlation exists between  $CTDI_{vol}$  normalized brain dose and both  
50 geometric and attenuation-based patient size metrics. A slightly lower correlation between  $CTDI_{vol}$   
normalized organ dose and patient size was observed for the lens of the eye. This may be due to the  
combination of the eye lens being a small peripheral organ and the presence of surface dose variation in both  
contiguous axial and helical scanning. Results indicate that robust estimates of patient-specific head CT dose  
may be provided using the size-specific, scanner-independent  $CTDI_{vol}$ -to-organ-dose **conversion coefficients**  
55 described in this work.

## I. Introduction

The number of CT procedures in the United States increased at an annual rate of over 10% between  
the years 1993-2006 to a total of 67 million CT scans performed in 2006.<sup>1</sup> **A total of 28.4% of these scans**  
were of the head.<sup>1</sup> A study looking at CT scans performed on patients younger than 22 years of age in Great  
60 Britain between 1985 and 2002 found that 64% of scans were of the head.<sup>2</sup> Furthermore, an analysis of  
patients at the University of New Mexico Health Science Center found that 39% of patient having head CT  
procedures had a prior head CT, the highest percentage among all regions of the body.<sup>3</sup> The high frequency  
of head CT procedures coupled with the fact that radiation exposure from CT scans has been identified as a  
significant component of the total medical radiation exposure globally warrants the need for accurate  
65 quantification of patient dose from head CT examinations.<sup>4</sup>

At present, radiation dose from a CT procedure is commonly quoted as the volume computed  
tomography dose index ( $CTDI_{vol}$ ) value displayed on the scanner console.<sup>5-8</sup>  $CTDI_{vol}$  was originally  
developed to allow for the characterization of scanner radiation output from different CT scanners and  
different technical parameter settings. Although scanner reported  $CTDI_{vol}$  takes into consideration scan  
70 parameters such as tube voltage, tube current, gantry rotation time, pitch, nominal beam collimation, actual

beam collimation and added bowtie filtration, it is measured for only a 16 cm and 32 cm diameter polymethyl methacrylate (PMMA) cylindrical phantom and therefore only represents a small subset of possible patient sizes. Because the patient dose from a CT exam is dependent upon both scanner radiation output and patient size,  $CTDI_{vol}$ , on its own, is not robust enough to accurately estimate patient dose.<sup>9</sup>

75

In an effort to get more utility out of  $CTDI_{vol}$ , Turner *et al.* showed that  $CTDI_{vol}$  could be used to effectively account for the differences among 64-slice multi-detector CT (MDCT) scanners from various manufacturers when estimating organ doses in patients undergoing abdominal CT examinations.<sup>10</sup> By normalizing Monte Carlo simulated organ dose by  $CTDI_{vol}$ , the variation of organ doses across scanners was reduced, on average, from 31.5% to 5.2%. The authors concluded that it was possible to generate scanner-

80 independent  $CTDI_{vol}$ -to-organ-dose **conversion coefficients** for each organ of interest and that these could be used to estimate organ dose to within 10% of dose values from detailed Monte Carlo simulations. It was then shown that  $CTDI_{vol}$  normalized organ doses and patient size correlated strongly in an exponential fashion.<sup>11</sup>

80

**AAPM Task Group 204 expanded upon this work and published a set of  $CTDI_{vol}$ -to-patient-dose conversion coefficients for a wide range of patient sizes when either the 16 cm or 32 cm  $CTDI$  phantom was used as the**

85 **reference phantom.<sup>12</sup> Various studies have shown that patient dose calculated using these conversion coefficients is a good surrogate for both pediatric and adult organ dose.<sup>13,14</sup>** The work of AAPM Task Group 204, though, was constrained to the determination of **conversion coefficients** for abdominal CT examinations only.

85

90

The purpose of this investigation is to further expand upon the work of AAPM Task Group 204 and generate patient-specific, scanner-independent  $CTDI_{vol}$ -to-organ-dose **conversion coefficients** for organs of interest irradiated during head CT examinations. This work concentrates on generating **conversion coefficients** through Monte Carlo simulation of head CT examinations for eight voxelized patient models of sizes ranging from infant to adult. Because of the large variability in tissue attenuation in the head, **conversion coefficients** were determined for both geometric and attenuation-based patient size metrics.

95 Given that there are advantages and disadvantages for both axial and helical scan modes,<sup>15</sup> the clinical default mode for head CT protocols varies between different manufacturers, scanners and facilities.

Therefore, **conversion coefficients** were determined for both scan modes.

## II. Materials and Methods

### II.A Patient Models

100 Organ doses were obtained through Monte Carlo simulations of eight patient models from the GSF family of voxelized phantoms.<sup>16,17</sup> The voxelized patient models were created from CT images, and within each model, upwards of 128 individual organs and anatomical structures were segmented from the images. This results in each patient model being represented as a three-dimensional matrix of organ identification numbers. In order to incorporate the patient models into our Monte Carlo simulations, each organ  
105 identification number was assigned a material description (i.e. weight fractions and density) based on anatomical tissue descriptions from ICRU Report 44.<sup>18</sup> Characteristics of the patient models are outlined in Table 1. Of the eight patient models, two are pediatric patients, three are adult males and three are adult females. All patient models were represented as being in the supine, headfirst position.

110 **Table 1.** Characteristics of the GSF family of voxelized phantoms used in this investigation.

Name	Gender	Age	Image columns	Image rows	Image slices	Column width (mm)	Row depth (mm)	Slice height (mm)
Baby	Female	8 weeks	267	138	142	0.85	0.85	4
Child	Female	7 yr	256	256	144	1.54	1.54	8
Helga	Female	26 yr	512	512	114	0.98	0.98	10
Irene	Female	32 yr	262	132	348	1.875	1.875	5
Golem	Male	38 yr	256	256	220	2.08	2.08	8
Visible Human	Male	38 yr	512	512	250	0.91	0.94	5
Donna	Female	40 yr	256	256	179	1.875	1.875	10
Frank	Male	48 yr	512	512	193	0.742	0.742	5

For each of the GSF patient models, the number of voxels representing the lens of the eye and the respective volume of the lens of the eye is outlined in Table 2. Although the voxel resolution of the GSF phantoms is too coarse to properly define the shape of the eye lenses, the eye lenses are at their correct anatomical location, frontal side of the eye bulb. For CT dosimetry, where the dose gradients are not too steep, this is sufficient detail. Concerns over the use of voxelized phantoms for lens of the eye dose assessment were outlined in Appendix F of ICRP 116.<sup>19</sup> In that report, the ICRP put emphasis on the dose to the thin layer of sensitive cells within the lens of the eye. This is in contrast to the dose to the whole lens of the eye, which is considered in this investigation. Short-ranged radiations such as beta and alpha particles were also considered in ICRP 116. For these radiations, the coarse lens of the eye representation is not sufficient, and therefore, stylized models had to be used instead. Such detail, though, is beyond the scope of CT dosimetry, and as such, using the GSF phantoms to assess dose to the lens of the eye can be justified without issue.

**Table 2.** Number of voxels representing the lens of the eye and volume of the lens of the eye for each GSF patient model

Name	Number of voxels	Volume (mm <sup>3</sup> )
Baby	69	199.4
Child	28	531.2
Helga	156	1498.2
Irene	84	1476.6
Golem	26	899.9
Visible Human	122	521.8
Donna	52	1828.1
Frank	288	627.6

## II.B Size Metrics

### II.B.1 Perimeter

As a first order approximation of patient size, head perimeter was measured at the first slice superior to the eyes for each patient model. In order to determine this geometric measure of size, a complete circumferential line was drawn around the head at the first slice superior to the eyes, and its length was recorded. This method is consistent with the head perimeter measurement technique outlined in the CDC anthropometry procedures manual.<sup>20</sup>

### II.B.2 Effective Diameter (ED)

Another geometric measure of patient size, effective diameter (ED), was calculated for each patient model using the method outlined in AAPM Report No. 204.<sup>12</sup> At the first slice superior to the eyes, the maximum anterior-posterior (AP) and lateral (LAT) dimensions were measured. Taking the square root of the product of the AP and LAT measurements, ED was uniquely determined for each patient model. For abdominal CT examinations, AAPM Task Group 204 tabulated CTDI<sub>vol</sub>-to-patient-dose conversion coefficients as a function of ED.<sup>12</sup>

### II.B.3 Water Equivalent Diameter (WED)

ED is a reasonable estimate of patient size for abdominal CT examinations because of the rather uniform tissue attenuation throughout that region. Given the variability in tissue attenuation within the head, it may be more appropriate to use an attenuation-based size metric to describe patient size for head CT examinations.<sup>21,22</sup>

A popular, reproducible attenuation-based patient size metric is water equivalent diameter (WED).<sup>23,24</sup> It has been shown that for CT dose estimation, the region of the body that was irradiated can be modeled as a cylindrical water phantom.<sup>25,26</sup> The WED is chosen such that the cylindrical water phantom has the same average x-ray attenuation as the region of the body that was irradiated. WED can be calculated directly from the CT images using the CT numbers that describe the CT pixel data. For a detailed explanation of how WED is calculated from CT images, please see Appendix A of Menke.<sup>23</sup> WED cannot be

determined directly from the GSF voxelized phantom data, since pixel data for these models is described in terms of organ identification numbers, not CT numbers. Instead, estimates of WED for each GSF patient model were determined through an indirect approach.

The WED estimates for the GSF models were obtained using correlations between WED and both ED and perimeter observed in an independent patient population. Image data of 42 patients of size ranging from infant to adult who received clinically indicated head CT scans was analyzed to calculate head perimeter, ED and WED. All geometric and attenuation-based size measurements were made at the first slice superior to the eyes. WED was calculated with the head segmented from the surrounding air and table.<sup>27</sup> Geometric size measurements for each patient, perimeter and ED, were then correlated with the corresponding calculation of WED. To obtain the estimated WED for each GSF patient model, the correlation function between WED and other patient size metrics was selected and the appropriate size metric (e.g. ED) for each model was used as input to that function. This approach allowed us to estimate WED using the geometric size measurements available for each GSF patient model.

## **II.C CT Scanners and Scanning Parameters**

64-slice MDCT scanners from four major manufacturers were included in this investigation: LightSpeed VCT (GE Healthcare, Waukesha, WI), Brilliance CT 64 (Philips Medical Systems, Cleveland, OH), Sensation 64 (Siemens Medical Solutions, Forchheim, Germany) and Aquilion 64 (Toshiba Medical Systems, Inc., Otawara-shi, Japan). Monte Carlo simulations of each scanner were performed using a tube voltage of 120 kVp, the widest available collimation setting (most dose efficient collimation), the bowtie filter designed for the adult head and, when the helical scan mode was simulated, a pitch of 1. While it is recognized that, clinically, a narrower collimation or a different bowtie filter for smaller patients may be used, scanner settings used in this investigation will allow for the simulations to be as comparable as possible across all scanners and will allow us to isolate the effect of patient size under constant source conditions.<sup>11</sup> Additionally, some scanners cannot actually perform a helical scan with a pitch of 1, but again, standardizing

the settings across all scanners will allow for analogous simulations. The Monte Carlo simulation package used in this investigation also models the actual longitudinal beam width of each scanner (previously measured with optically stimulated luminescence strips). Table 3 outlines the nominal collimation and actual longitudinal beam width used for each scanner.

**Table 3.** Collimation settings used for simulations of scanners included in this investigation. Detector configuration for each collimation given in brackets [].

Manufacturer	Scanner	Nominal beam width (mm)	Actual beam width (mm)
GE	LightSpeed VCT	40 [64 x 0.625]	42.4
Philips	Brilliance 64	40 [64 x 0.625]	43.7
Siemens	Sensation 64	28.8 [24 x 1.2]	32.2
Toshiba	Aquilion 64	32 [64 x 0.5]	36.9

## II.D CTDI<sub>vol</sub> Measurements

Using the technical settings outlined in Section II.C, conventional CTDI<sub>100</sub> exposure measurements were made at the center and periphery (12 o'clock) positions of the head (16 cm in diameter) CTDI phantom. All measurements were made with a standard 100 mm pencil ionization chamber and calibrated electrometer. All measured exposures in milliroentgen (mR) were converted to dose to air in mGy using 1 mR = 0.00876 mGy. A rotation time of 1 s and a tube current of 300 mA were set to ensure reproducible measurements across all scanners. CTDI<sub>vol</sub> was calculated from the CTDI<sub>100</sub> measurements and recorded on a per tube current time product basis (mGy/mAs).<sup>8</sup>

## II.E Monte Carlo Simulations

### II.E.1 Overview

The Monte Carlo software package MCNPX (Monte Carlo N-Particle eXtended version 2.7.0) was used as the simulation engine for this investigation.<sup>28</sup> Within all the simulations, the detailed photon transport mode with a low-energy cutoff of 1 keV was used. The detailed physics treatment includes coherent scattering and accounts for fluorescent photons after photoelectric absorption. Form factors and Compton profiles are used to account for electron binding effects, and analog capture is always used. The incoherent, coherent and photoelectric cross section data is based on ENDF/B-VII.<sup>29</sup> Simulation physics options are set so that the photon transport mode does not explicitly create photoelectrons but instead assumes all secondary electrons deposit their energy at the photon interaction site, which is reasonable given the incident photon energy distribution for a 120 kVp beam. This assumption satisfies charged particle equilibrium and allows absorbed dose to be approximated as collision kerma, which was calculated in each volume of interest by tallying the photon energy fluence and multiplying by the material-specific and energy-dependent mass energy-absorption coefficient. The mass energy-absorption coefficients used in this investigation are referenced from Hubbell and Seltzer.<sup>30</sup>

Normalization factors are required to convert simulated dose values (mGy per particle) to absolute dose normalized on a tube current time product basis (mGy per total mAs). In order to do this, air scan measurements (mGy per total mAs) and corresponding simulations (mGy per particle) were performed using the appropriate beam energy and nominal collimation for each scanner listed in Table 3. Again, measured exposures in mR were converted to dose to air in mGy using  $1 \text{ mR} = 0.00876 \text{ mGy}$ . For air scan measurements, the 100 mm pencil ionization chamber was attached to the patient table such that the active portion of the chamber was extended beyond the edge of the table at the scanner isocenter and therefore essentially “free-in-air.” A CTID<sub>100</sub> in air measurement was then made. A corresponding simulation using an ionization chamber model at isocenter was then performed in MCNPX. By dividing the air scan measurement by the air scan simulation, a normalization factor (particles per total mAs) was uniquely determined for each scanner, similar to that described by DeMarco *et al.*<sup>31</sup> Dose simulation results were then multiplied by the appropriate normalization factor to yield simulated dose in units of mGy per total mAs.

Although normalization factors can be calculated using measurements and simulations within some phantom, the advantage of air scan normalization factors is that the chamber position is reproducible in a locally homogeneous dose region void of any nearby attenuating mediums such as the patient table.<sup>32</sup>

## 225 II.E.2 CT Source Model

Modifications were made to the standard MCNPX source code in order to be able to randomly sample from all possible starting positions corresponding to a contiguous axial or helical scan performed for a given nominal beam collimation, scan length and, for helical scanning, pitch. Further modifications of the MCNPX source code allowed for scanner-specific fan angles and measured beam widths (as opposed to  
230 nominal beam collimations) to be accounted for when sampling photon trajectories. An equivalent source model previously described by Turner *et al.* was used to generate scanner-specific spectrum and bowtie filter descriptions for each scanner in this investigation.<sup>33</sup> For a given scanner, the energy of each simulated photon is obtained by sampling the scanner-specific energy spectrum. Attenuation due to the bowtie filter is modeled by adjusting the statistical weighting factor of each photon. The bowtie filter description is used to  
235 determine the path length each simulated photon traverses through the bowtie filter as a function of the photon's trajectory. Using the path length and the linear attenuation coefficients of aluminum, the resulting exponential attenuation factor is calculated. Multiplying this exponential attenuation factor by an initial particle weight of 1 yields the new weighting factor for that photon in MCNPX.

The equivalent source model was previously validated for all scanners considered in this  
240 investigation by comparing simulated and physically measured CTDI<sub>100</sub> at the center and periphery of both 32 and 16 cm CTDI phantoms. An average root-mean-square error of approximately 5% between the simulated and measured values was reported.<sup>33</sup>

## II.E.3 Head CT Simulations

Simulated contiguous axial and helical head scans were performed for each GSF patient model listed

245

in Table 1. As per the recommendations found in the AAPM Routine Head CT Protocols version 1.1, the scan range was set from the top of the C1 lamina through the top of the calvarium.<sup>15</sup> Table 4 outlines the scan length for each patient model. For each simulation, absorbed dose to both the brain and lens of the eye was tallied using the method outlined in Section II.E.1. **Ten million photon histories** were used to achieve a statistical uncertainty of less than 1% for each simulation.

250

Because of differences in nominal beam collimation (Table 3), each scanner will require a varying number of rotations to complete the scan lengths outlined in Table 4. This will result in differences in total mAs across scanners for a given scan length (total mAs = mAs per rotation x number of rotations). In order to account for these differences, organ doses were converted to units of mGy per mAs (where mAs refers to mAs per rotation) by multiplying the simulation results in mGy per total mAs by the total number of

255

rotations used in the corresponding contiguous axial or helical simulation.

**Table 4.** Scan length from top of C1 lamina through top of calvarium for each GSF patient model.

Name	Scan length (cm)
Baby	10.20
Child	14.80
Helga	14.50
Irene	15.75
Golem	15.60
Visible Human	15.25
Donna	15.50
Frank	21.75

260

While it is recognized that tucking the patient's chin (tuck) and/or tilting the gantry (tilt) are commonly employed in head CT scanning as methods to reduce lens of the eye exposure, tuck and tilt were not simulated as part of this investigation. This is because we want to focus exclusively on dose to organs

that are fully irradiated. Because tuck and tilt will cause varying levels of partial irradiation (or non irradiation) of the lens of the eye across the different patient models, eliminating tuck and tilt from the simulations allowed us to isolate the effects of patient size on  $CTDI_{vol}$  normalized organ dose. In addition, if tuck or tilt was used and the lens of the eye was not exposed, quantifying organ dose may no longer be a concern in that situation. For dose to the brain, it is expected that the majority of it would be completely irradiated regardless of whether tuck and/or tilt was used.

## II.F Organ Dose Estimate Analysis

### II.F.1 Size-Specific, Scanner-Independent Organ Dose

Adopting nomenclature similar to that introduced by Turner *et al.*,<sup>10,11</sup> brain and lens of the eye dose resulting from simulations of each scanner, scan mode and patient model is denoted as  $D_{S,SM,P,O}$ , where  $S$  refers to the scanner,  $SM$  refers to the scan mode,  $P$  refers to the patient model and  $O$  refers to the organ.

Each organ dose was normalized by the measured  $CTID_{vol}$  values corresponding to the simulated scanner.

The  $CTDI_{vol}$  normalized organ dose is denoted as  $nD_{S,SM,P,O}$ . Because both organ dose and measured  $CTDI_{vol}$  are quoted in units of mGy per mAs, this normalization resulted in a unitless value. In order to derive a single value that accounts for the differences among the various scanners when estimating organ doses,  $nD_{S,SM,P,O}$  was averaged across all scanners for each combination of scan mode, patient model and organ.

This scanner-independent organ dose value is denoted as  $\overline{nD}_{SM,P,O}$ .

To explore the relationship between scanner-independent,  $CTDI_{vol}$  normalized organ dose,  $\overline{nD}_{SM,P,O}$ , and patient size, correlations between  $\overline{nD}_{SM,P,O}$  and the three patient size metrics outlined in Section II.B were calculated. Regression equations describing these correlations served as the means to generate scanner-independent organ dose estimates for any patient size (patient-specific, scanner-independent  $CTDI_{vol}$ -to-organ-dose conversion coefficients). In order to gauge the strength of these correlations for each patient size metric, correlation coefficients were tabulated for each combination of scan mode and organ.

## II.F.2 Organ Comparison

The brain and the lens of the eye are drastically different organs in terms of size and location. The brain is large and at depth. The lens of the eye, on the other hand, is small and superficial. In the work by Turner *et al.*,<sup>10,11</sup> only large abdominal organs at depth were examined. In order to determine if organ size and location affects the magnitude of scanner-independent organ dose estimates, scanner-independent brain and lens of the eye dose were compared for each scan mode.

## II.F.3 Scan Mode Comparison

In the work by Turner *et al.*,<sup>10,11</sup> only helical scan simulations were evaluated. This was sufficient given that nearly all abdominal CT examinations are performed using the helical scanning mode. For head CT, though, there is a mix of contiguous axial and helical scanning in clinical practice. In order to determine if there is any scan mode dependence in scanner-independent organ dose estimates, contiguous axial and helical scanner-independent organ dose were compared for each organ.

## III. Results

### III.A Patient Size Metrics

For the 42 patients analyzed as part of the indirect determination of WED for the GSF models, a best-fit linear relationship was observed between ED and WED. Figure 1 shows the ED and WED data with the linear regression equation and correlation coefficient of 0.87. The WED of each GSF patient model was estimated using this linear regression equation with the measured ED values.

**Table 5** summarizes the three patient size metrics determined for each GSF model as part of this investigation: perimeter, ED and WED.

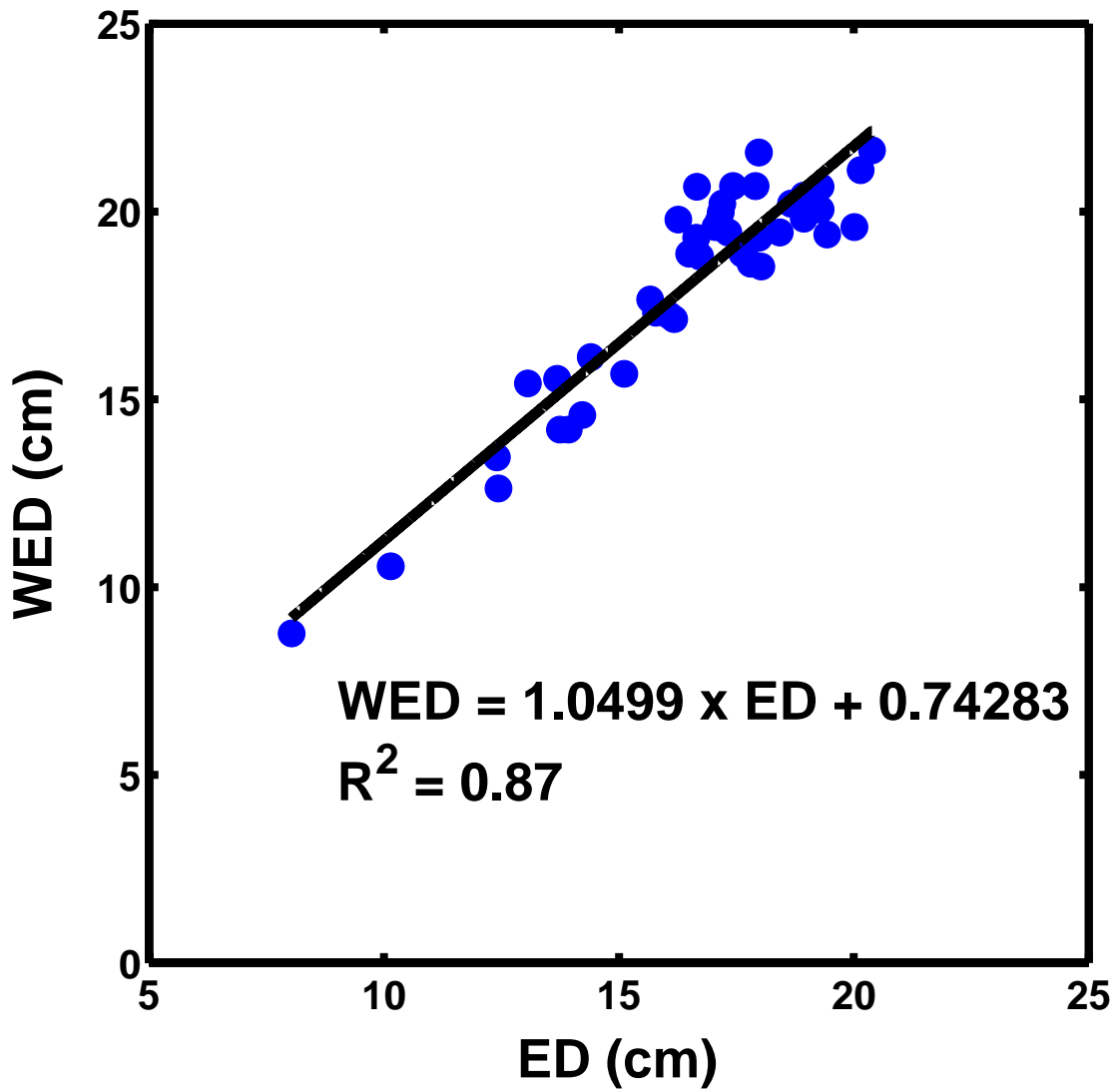


**Figure 1.** Correlation between ED and WED measured for 42 patients ranging from infant to adult.

**Table 5.** Perimeter, ED and WED determined for each GSF patient model.

Name	Perimeter (cm)	ED (cm)	WED (cm)
Baby	32.67	9.84	11.07
Child	50.50	15.68	17.21
Helga	56.20	16.60	18.17
Irene	52.52	15.58	17.10
Golem	56.09	16.74	18.32
Visible Human	61.89	18.25	19.90
Donna	55.82	17.14	18.74
Frank	57.11	17.57	19.19

### III.B Size-Specific, Scanner-Independent Organ Dose Estimates

Table 6 shows  $\overline{nD}_{SM,P,O}$  for the brain and lens of the eye for each GSF patient model for both contiguous axial and helical scan modes. Figure 2 shows  $\overline{nD}_{SM,P,O}$  for the brain and lens of the eye as a function of each of the three patient size metrics for both contiguous axial and helical scan modes. An exponential relationship between  $\overline{nD}_{SM,P,O}$  and patient size was observed for all patient size metrics, scan modes and organs. **This is expected given the exponential relationship between x-ray beam intensity and patient size.** These exponential relationships are described by an exponential regression equation of the form

$$\overline{nD}_{SM,P,O} = A_0 \exp(B_0 \times \text{Patient Size})$$

(1)

where  $A_0$  and  $B_0$  are exponential regression coefficients specific to the combination of scan mode and organ. The exponential regression coefficients and correlation coefficients ( $R^2$ ) for each combination of organ and patient size metric for the contiguous axial scan mode are shown in Table 7. **Table 8** shows analogous information for the helical scan mode. For the brain, correlation coefficients ranged from 0.92 to 0.93. For the lens of the eye, correlation coefficients ranged from 0.73 to 0.85.

**Table 6.** Scanner-independent organ dose values for both contiguous axial and helical scan modes for each GSF model.

Name	Contiguous axial		Helical	
	Brain (mGy/CTDI <sub>vol</sub> )	Lens of the eye (mGy/CTDI <sub>vol</sub> )	Brain (mGy/CTDI <sub>vol</sub> )	Lens of the eye (mGy/CTDI <sub>vol</sub> )
Baby	1.22	1.30	1.09	1.06
Child	0.86	0.95	0.78	0.83
Helga	0.77	0.86	0.69	0.79
Irene	0.75	0.91	0.68	0.77
Golem	0.76	0.96	0.71	0.82
Visible Human	0.68	0.88	0.62	0.78

Donna	0.72	0.75	0.66	0.75
Frank	0.65	0.90	0.60	0.80

330

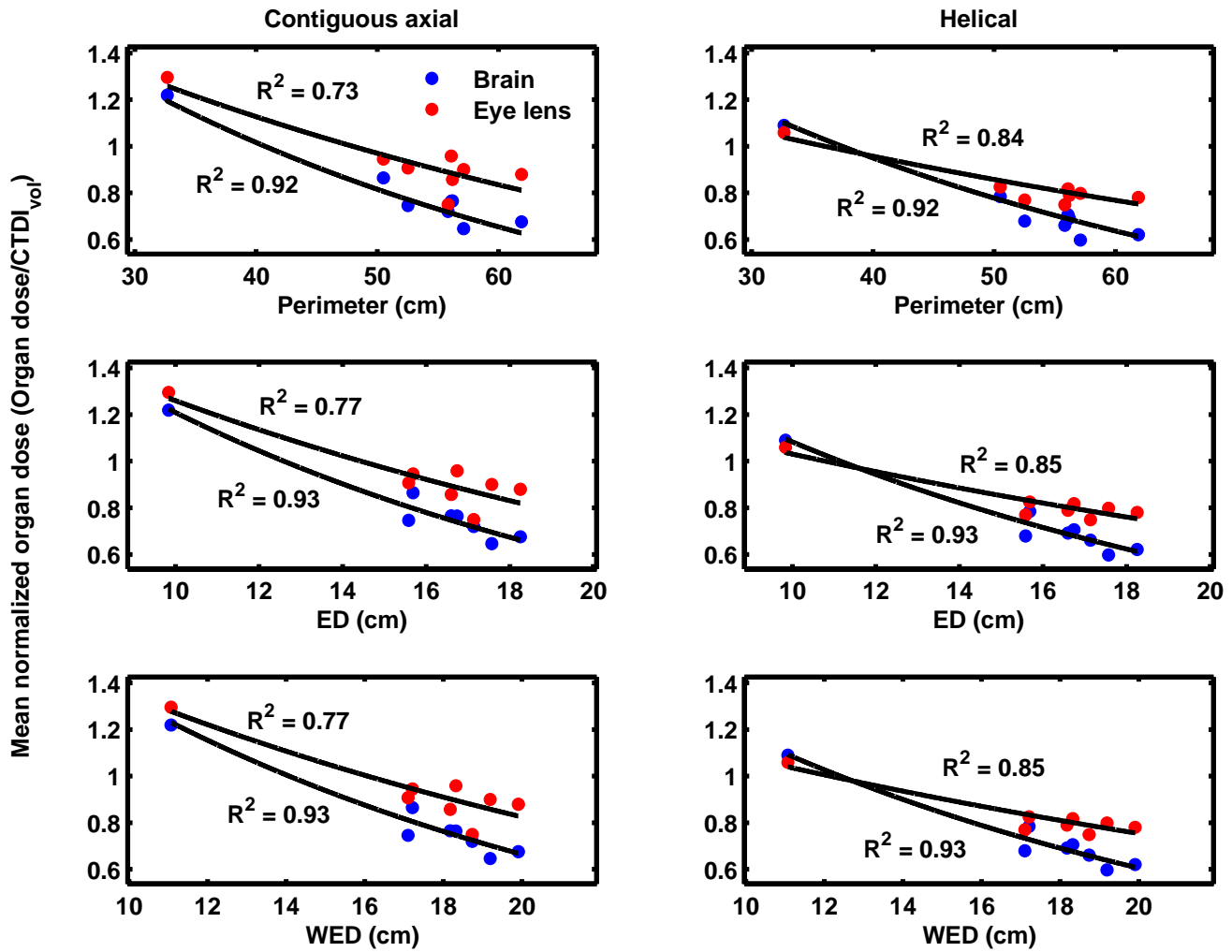


**Figure 2.** Mean CTDI<sub>vol</sub> normalized brain and lens of the eye dose as a function of each of the three patient size metrics for both contiguous axial (left) and helical (right) scan modes.

335

**Table 7.** Exponential regression coefficients and correlation coefficients for each combination of organ and patient size metric for the contiguous axial scan mode.

Patient size metric	Brain			Lens of the eye		
	A <sub>0</sub>	B <sub>0</sub>	R <sup>2</sup>	A <sub>0</sub>	B <sub>0</sub>	R <sup>2</sup>
Perimeter	2.451	-0.022	0.92	2.054	-0.015	0.73
ED	2.509	-0.073	0.93	2.119	-0.052	0.77
WED	2.641	-0.069	0.93	2.198	-0.049	0.77

340

**Table 8.** Exponential regression coefficients and correlation coefficients for each combination of organ and patient size metric for the helical scan mode.

Patient size metric	Brain			Lens of the eye		
	$A_0$	$B_0$	$R^2$	$A_0$	$B_0$	$R^2$
Perimeter	2.115	-0.020	0.92	1.487	-0.011	0.84
ED	2.159	-0.069	0.93	1.507	-0.038	0.85
WED	2.268	-0.066	0.93	1.549	-0.036	0.85

### III.C Organ Comparison

345

The data from Table 6 was used to calculate differences between scanner-independent brain and lens of the eye dose across all patient models for each scan mode. The difference between  $\overline{nD}_{SM,P,O}$  for the brain and lens of the eyes for the contiguous axial scan mode ranged from 4.1 to 39.3% (mean = 18.5%, SD = 12.6%). For the helical scan mode, the difference ranged from 2.9 to 33.5% (mean = 15.5%, SD = 10.0%). A qualitative representation of these differences can be seen in Figure 2.

### III.D Scan Mode Comparison

350

The data from Table 6 was also used to calculate the differences between contiguous axial and helical scanner-independent organ dose across all patient models for both the brain and lens of the eye. For the brain, the difference between  $\overline{nD}_{SM,P,O}$  for the contiguous axial and helical scan modes ranged from 8.1-11.8% (mean = 9.6%, SD = 1.3%). For the lens of the eye, the difference ranged from 0.1-22.3% (mean = 13.3%, SD = 6.7%). Figure 3 shows  $\overline{nD}_{SM,P,O}$  for the contiguous axial and helical scan modes as a function of each of the three patient size metrics for both the brain and lens of the eye.

355

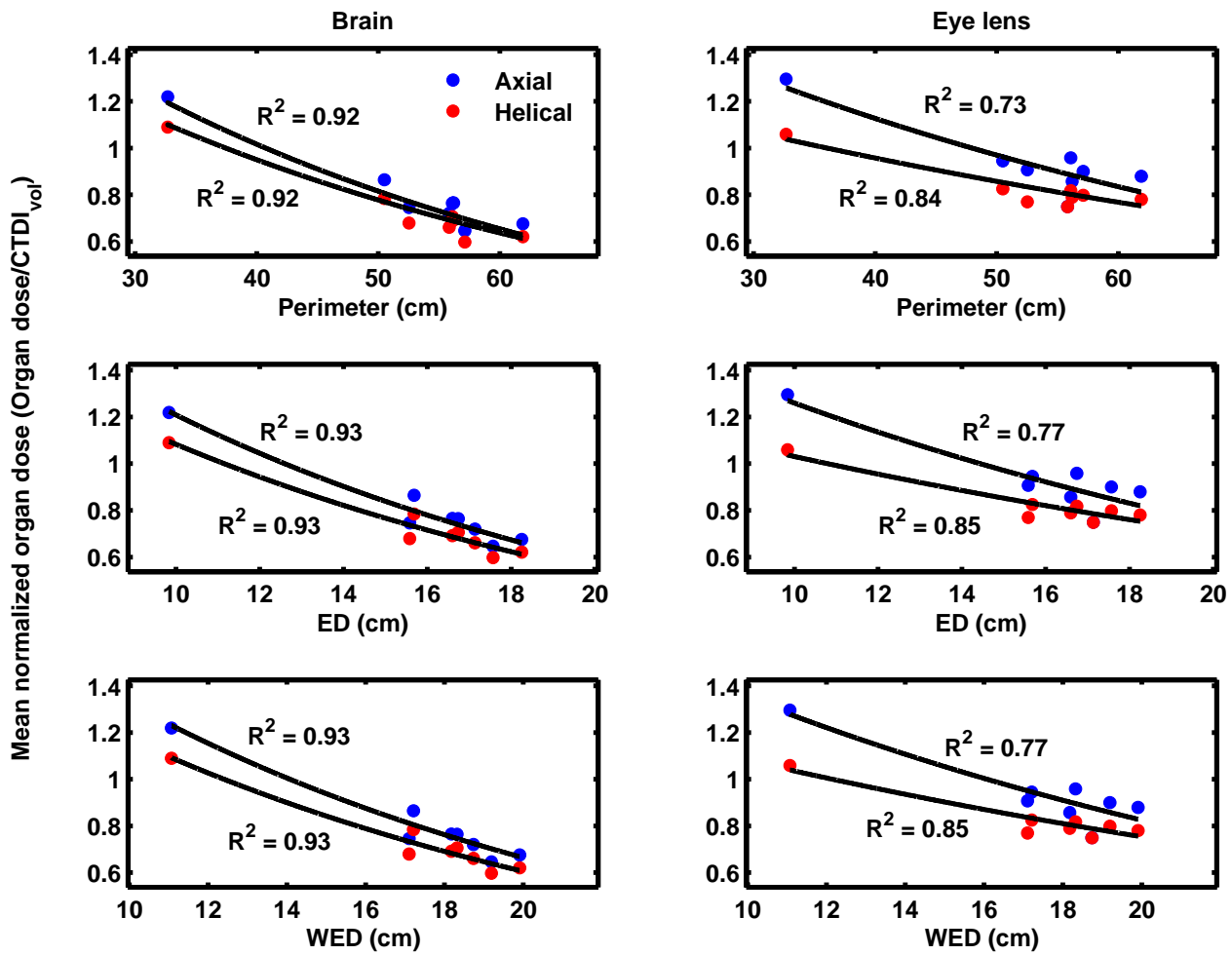


**Figure 3.** Contiguous axial and helical mean  $CTDI_{vol}$  normalized organ dose as a function of each of the three patient size metrics for both the brain (left) and lens of the eye (right).

#### 360 IV. Discussion and Conclusions

For the brain, correlation coefficients ranging from 0.92 to 0.93 indicate that each patient size metric described here can serve as an excellent predictor of  $\overline{nD}_{SM,P,O}$  for the brain. For the lens of the eye, correlation coefficients ranging from 0.73 to 0.85 provide evidence that these patient size metrics are likewise a very good predictor of  $\overline{nD}_{SM,P,O}$  for the lens of the eye but also indicate that other factors not considered in this investigation may have contributed to the magnitude of the correlations.

365

Work by Zhang *et al.* previously showed substantial surface dose variation for helical scans over a range of pitch values as well as contiguous axial scans.<sup>34</sup> Variation in peripheral dose patterns was shown to be upwards of 45% and 30% for contiguous axial and helical (pitch of 1) scans, respectively.<sup>34</sup> These effects were demonstrated to be affected by wider beam collimations and tube start angle effects. Given that weaker correlations between  $\overline{nD}_{SM,P,O}$  and patient size were seen for the small, superficial lens of the eye, surface dose variation more than likely played a role in the determination of  $\overline{nD}_{SM,P,O}$ . Both nominal and actual beam width are accounted for in  $CTDI_{vol}$ , so hypothetically,  $\overline{nD}_{SM,P,O}$  should be robust enough to be applied for any scanner collimation. Results from this work, though, indicate that may only be true for large organs at depth (i.e brain or most abdominal organs). In addition, because  $CTDI_{vol}$  is measured using a single axial scan, tube start angle effects are not built directly into it. Averaging  $\overline{nD}_{SM,P,O}$  across a variety of start angles may be the best way to approximate these effects in a single  $\overline{nD}_{SM,P,O}$  value. In this investigation, the tube start angle was at the 12 o'clock position for all helical simulations. Future investigations will focus on quantifying the impact of some of the factors that influence surface dose variations (including helical pitch values, which most manufacturers are now recommending pitch values  $< 1$  for helical head scans, as well variation in tube start angle and nominal beam collimation) on  $\overline{nD}_{SM,P,O}$  for surface organs like the lens of the eye.

As shown in Figure 2 and quantified in Section III.C, for a given patient size, variation between  $\overline{nD}_{SM,P,O}$  for the brain and lens of the eye was upwards of 39.3% and 33.5% for the contiguous axial and helical scan modes, respectively. Turner *et al.* and AAPM Task Group 204 showed that dose to any fully irradiated organ in the abdomen could be approximated using a single  $\overline{nD}_{SM,P,O}$  value.<sup>11,12</sup> Results from this investigation show that may only have been true because organs of interest in the abdomen are all relatively large and at depth within the body. When considering small, superficial organs, surface dose variation plays a large role in the determination of  $\overline{nD}_{SM,P,O}$ , and thus individual  $\overline{nD}_{SM,P,O}$  values for the brain and lens of

the eye may be necessary in order to derive the most accurate organ-specific dose estimates for all patient sizes.

Previous studies have shown a distinct difference between doses from contiguous axial and helical scans of the same scan length.<sup>35-37</sup> These studies were all based on physically measured dose. Within this work, we have also shown these differences to be present in Monte Carlo simulations. As quantified in Section III.D, for the brain, the difference between  $\overline{nD}_{SM,P,O}$  for contiguous axial and helical scan modes is upwards of 11.8%. For the lens of the eye, the difference is as much as 22.3%. The difference between doses for contiguous axial and helical scans was previously speculated to be due to differences in tube on-time characteristics between contiguous axial and helical scan modes,<sup>37</sup> but because we also see this effect in Monte Carlo simulations, this doesn't appear to be the answer. The magnitude of the difference for the lens of the eye relative to that for the brain indicates that surface dose variation may be a large contributor to the difference in dose between the scan modes. As such, in order to provide the most accurate dose estimates,  $\overline{nD}_{SM,P,O}$  values unique to each scan mode should be used rather than a single set of  $\overline{nD}_{SM,P,O}$  values that apply to both contiguous axial and helical scanning.

Because of the fairly uniform head size of adults, as shown in Table 5, patients with WED less than 17 cm are not well represented by the GSF patient models. This size range includes pediatric and small adult patients, so it's important to validate that  $\overline{nD}_{SM,P,O}$  values described in this work are applicable to these patients. A set of 5 pediatric patients with WED ranging from 8.77 to 15.55 cm was selected from the group of patients analyzed as part of the indirect determination of WED for the GSF models, as described in Section III.A. Using the CT images of these patients, voxelized patient models were created, the brain was segmented and Monte Carlo simulations of brain dose were performed for each of the scanners described in Section II.C. Figure 4 shows  $\overline{nD}_{SM,P,O}$  calculated for each pediatric patient and GSF model as a function of WED. For each of the pediatric patients, the difference between  $\overline{nD}_{SM,P,O}$  determined using detailed Monte

Carlo simulations and  $\overline{nD}_{SM,P,O}$  determined using the exponential regression equation, which was derived from the GSF data only, ranged from 0.15% to 7.84%. These preliminary results from organ-specific dose simulations performed using actual patient images indicate that the  $CTDI_{vol}$ -to-organ-dose conversion coefficients presented in this work can be effectively applied for patients with WED less than 17 cm. A more extensive analysis of dose from simulations of actual patient images will be addressed in future investigations.

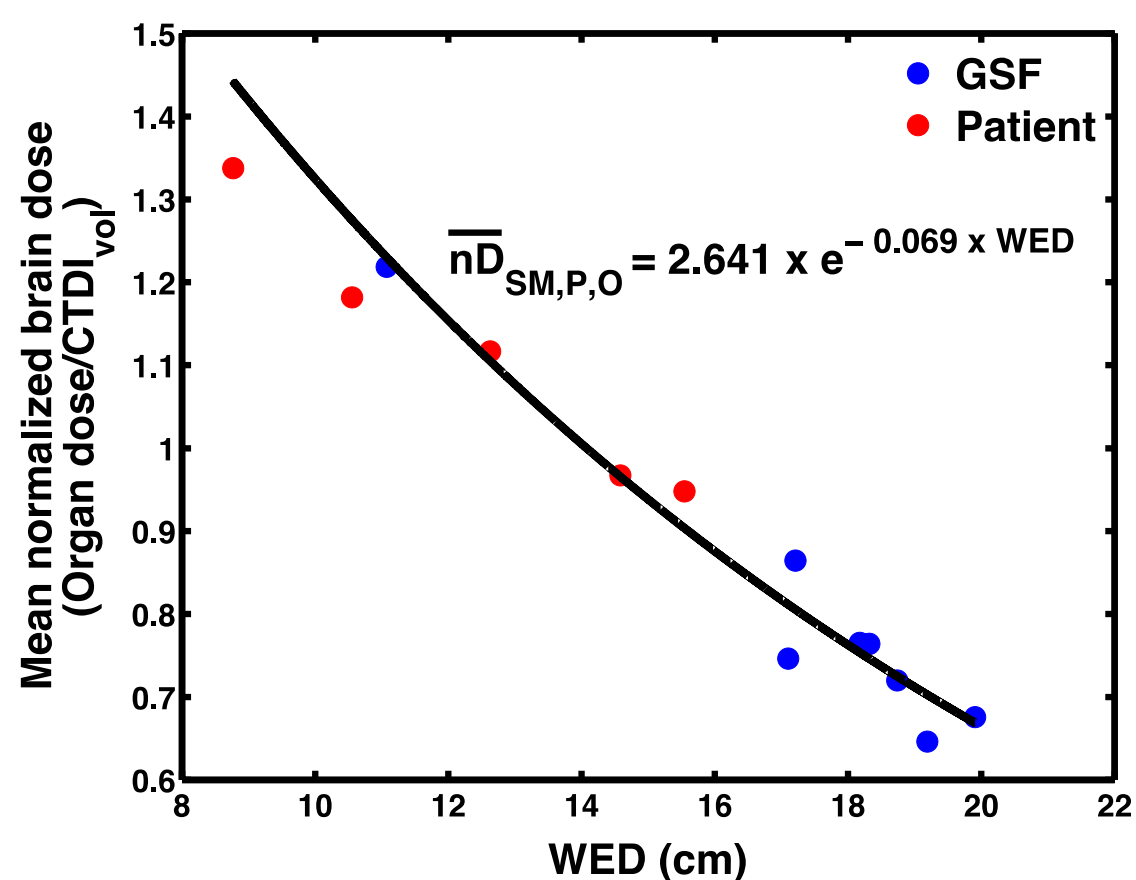


**Figure 4.** Contiguous axial mean  $CTDI_{vol}$  normalized brain dose as a function of WED for both pediatric patient and GSF models. Exponential fit shown is based on Equation 1 with exponential regression coefficients from Table 7.

It should be emphasized that the  $CTDI_{vol}$ -to-organ-dose conversion coefficients presented in this work are only appropriate for “routine” head CT exams where there is full coverage of the brain and lens of the eye.<sup>15</sup> These conversion coefficients should not be used for sinus scans or other protocols that result in

partial irradiation of the brain or lens of the eye. Like tucking the patient's chin and/or tilting the gantry, protocols other than those that yield full coverage of the brain and lens of the eye will cause varying levels of partial irradiation (or non irradiation) of the brain and lens of the eye across the different patient models, thus limiting our ability to isolate the effects of patient size on CTDI<sub>vol</sub> normalized organ dose. While it is recognized that dose to partially irradiated organ is a prominent issue in CT dosimetry, it is outside the scope of this work and will be addressed in future investigations.

Using the exponential regression coefficients outlined in Tables 6 and 7 in conjunction with Equation 1, patient-specific, scanner-independent CTDI<sub>vol</sub>-to-organ-dose conversion coefficients can be generated for the brain and lens of the eye for any patient size determined using a variety of geometric and attenuation-based size metrics. Multiplying these conversion coefficients by the CTDI<sub>vol</sub> (16 cm reference phantom) of the scan of interest yields robust estimates of patient-specific, organ-specific dose for head CT examinations.

## Acknowledgements

This work was supported by a grant from Siemens Medical Solutions through a Master Research Agreement with UCLA Department of Radiological Sciences.

## References

1. F. A. Mettler *et al.*, "Medical Radiation Exposure in the U.S. in 2006: Preliminary Results," *Health Phys.* **95**, 502-507 (2008).
2. M. S. Pearce *et al.*, "Radiation exposure from CT scans in childhood and subsequent risk of leukaemia and brain tumours: a retrospective cohort study," *Lancet.* **380**, 499-505 (2012).
3. F. A. Mettler, P. W. Wiest, J. A. Locken, C. A. Kelsey, "CT scanning: patterns of use and dose," *J. Radiol. Prot.* **20**, 353-359 (2000).
4. National Council on Radiation Protection and Measurements, "Ionizing radiation exposure of the population of the United States," NCRP Report No. 160 (2009).
5. C. H. McCollough, "CT Dose: How to measure, how to reduce," *Health Phys.* **95**, 508-517 (2008).
6. R. L. Dixon, "A new look at CT dose measurement: Beyond CTDI," *Med. Phys.* **30**, 1272-1280 (2003).
7. J. M. Boone, "The trouble with CTDI<sub>100</sub>," *Med. Phys.* **34**, 1364-1371 (2007).
8. M. F. McNitt-Gray, "AAPM/RSNA physics tutorial for residents: Topics in CT – Radiation dose in CT," *Radiographics* **22**, 1541-1553 (2002).
9. C. H. McCollough, *et al.*, "CT dose index and patient dose: they are not the same thing," *Radiology* **259**, 311-316 (2011).

10. A. C. Turner *et al.*, "The feasibility of a scanner-independent technique to estimate organ dose from MDCT scan: Using CTDI<sub>vol</sub> to account for differences between scanner," *Med. Phys.* **37**, 1816-1825 (2010).
11. A. C. Turner *et al.*, "The feasibility of patient size-corrected, scanner-independent organ dose estimates for abdominal CT exams," *Med. Phys.* **38**, 820-829 (2011).
12. AAPM Task Group 204, "Size-Specific Dose Estimates (SSDE) in Pediatric and Adult Body CT Examinations," AAPM Report No. 204 (2011).
13. B. M. Moore, S. L. Brady, A. E. Mirro, R. A. Kaufman, "Size-specific dose estimates (SSDE) provides a simple method to calculate organ dose for pediatric CT examinations," *Med. Phys.* **41** 071917 (2014).
14. M. Supanich, D. Peck, "Size-specific dose estimates as an indicator of absorbed organ dose in CT abdomen and pelvis studies," *Radiological Society of North America 2012 Scientific Assembly and Annual Meeting, Chicago, IL* (2012).
15. AAPM, "Adult Routine Head CT Protocols Version 1.1," AAPM (2012).
16. N. Petoussi-Henss, M. Zankl, U. Fill, D. Regulla, "The GSF family of voxel phantoms," *Phys. Med. Biol.* **47**, 89-106 (2002).
17. U. A. Fill, M. Zankl, N. Petoussi-Henss, M. Siebert, D. Regulla, "Adult female voxel models of different stature and photon conversion coefficients for radiation protection," *Health Phys.* **86**, 253-272 (2004).
18. The International Commission on Radiation Units and Measurements, "Tissue substitutes in radiation dosimetry and measurement," ICRU Report No. 44 (1989).
19. The International Commission on Radiological Protection, "Conversion Coefficients for Radiological Protection Quantities for External Radiation Exposures," ICRP Publication 116 (2010).
20. Centers for Disease Control and Prevention, "National Health and Nutrition Examination Survey (NHANES): Anthropometry Procedures Manual," Centers for Disease Control and Prevention (2007).
21. J. Wang *et al.*, "Attenuation-based estimation of patient size for the purpose of size specific dose estimation in CT. Part 1. Development and validation of methods using CT image," *Med. Phys.* **39**, 6764-6771 (2012).
22. J. Wang *et al.*, "Attenuation-based estimation of patient size for the purpose of size specific dose estimation in CT. Part II. Implementation on abdomen and thorax phantoms using cross section CT images and scanned projection radiograph images," *Med. Phys.* **39**, 6772-6778 (2012).
23. J. Menke, "Comparison of different body size parameters for individual dose adaptation in body CT of adults," *Radiology* **236**, 565-571 (2005).
24. W. Huda, A. Vance, "Patient radiation doses from adult and pediatric CT," *AJR Am. J. Roentgenol.* **188**, 540-546 (2007).
25. W. Huda, E. M. Scalzetti, M. Roskopf, "Effective doses to patients undergoing thoracic computed tomography examinations," *Med. Phys.* **27**, 838-844 (2000).
26. W. Huda, J. V. Atherton, D. E. Ware, W. A. Cummings, "An approach for the estimation of effective radiation dose at CT in pediatric patients," *Radiology* **203**, 417-422 (1997).
27. The International Commission on Radiation Units and Measurements, "Radiation Dose and Image-Quality Assessment in Computed Tomography," ICRU Report No. 87 (2012).
28. D. B. Pelowitz, "MCNPX User's Manual Version 2.7.0," Los Alamos National Laboratory Report LA-CP-11-00438 (2011).
29. M. B. Chadwick *et al.*, "ENDF/B-VII.1: Nuclear Data for Science and Technology: Cross Sections, Covariances, Fission Product Yields and Decay Data," *Nuclear Data Sheets* **112**, 2887-2996 (2011).
30. J. H. Hubbell and S. M. Seltzer, "Tables of x-ray mass attenuation coefficients and mass energy-absorption coefficients," available at: <http://physics.nist.gov/PhysRefData/XrayMassCoef/cover.html> (2004).
31. J. J. DeMarco *et al.*, "A Monte Carlo based method to estimate radiation dose from multidetector CT (MCDT): cylindrical and anthropomorphic phantoms," *Phys. Med. Biol.* **50**, 3989-4004 (2005).
32. G. Zhang *et al.*, "Monte Carlo modeling for dose assessment in cone beam CT for oral and maxillofacial applications," *Med. Phys.* **40**, 072103 (2013).

33. A. C. Turner *et al.*, "A method to generate equivalent energy spectra and filtration models based on measurement for multidetector CT Monte Carlo dosimetry simulations," *Med. Phys.* **36**, 2154-2164 (2009).
- 510 34. Zhang *et al.*, "Variability of surface and center position radiation dose in MDCT: Monte Carlo simulations using CTDI and anthropomorphic phantoms," *Med. Phys.* **36**, 1025-1038 (2009).
35. A. McDermott, R. A. White, M. McNitt-Gray, E. Angel, D. Cody, "Pediatric organ dose measurements in axial and helical multislice CT," *Med. Phys.* **36**, 1494-1499 (2009).
- 515 36. L. L. Chang, F. D. Chen, P. S. Chang, C. C. Liu, H. L. Lien, "Assessment of dose and risk to the body following conventional and spiral computed tomography," *Zhonghua Yo Xue Za Zhi (Taipei)* **55**, 283-289 (1995).
37. A. G. Pitman, R. S. Budd, A. F. McKenzie, "Radiation dose in computed tomography of the pelvis: Comparison of helical and axial scanning," *Australas Radiol.* **41**, 329-335 (1997).